



Identification of the bridge moving loads based on fractional conjugate gradient method

Hongchun Wu¹ · Linjun Wang¹ · Chengsheng Luo¹

Received: 29 January 2024 / Accepted: 30 July 2024 / Published online: 28 August 2024

© The Author(s), under exclusive licence to The Brazilian Society of Mechanical Sciences and Engineering 2024

Abstract

This paper proposes a bridge moving load identification method based on the fractional conjugate gradient (FCG) method to address the low identification accuracy of traditional conjugate gradient methods. Firstly, the mathematical framework for detecting the moving load in the vehicle-bridge system is established by utilizing both the time-domain deconvolution technique and modal superposition approach. Secondly, the derivation of the discrete moving load identification system matrix equation enables its formulation as an unconstrained optimization problem. Finally, the load information is obtained iteratively by the FCG method. Experimental results demonstrate that, compared with the Hestenes–Stiefel conjugate gradient (HSCG) method, the Fletcher–Reeves conjugate gradient (FRCG) method, and the Polak–Ribire–Polyak conjugate gradient (PRPCG) method, the FCG method has faster identification speed, smaller identification error, and higher identification accuracy and noise resistance in identifying bridge moving loads at different noise levels.

Keywords Moving load identification · Fractional order · Conjugate gradient method · Noise immunity

1 Introduction

The safety and reliability of bridge structures are directly related to the development of society and the economy as a whole. With the rapid development of the national economy, traffic volume increasing, vehicle high-speed driving, and overloading during service, it can adversely affect the safety of bridges and also pose a significant threat to their integrity and stability [1–3]. In the field of bridge engineering, identifying and monitoring moving loads effectively and studying the impact of bridge vibration and damage on operational performance have become urgent and important problems that need to be solved [4–6]. Since the problem of self-loading identification is first introduced, scholars have conducted extensive research and achieved numerous results. Law et al. proposed an

improved time-domain method (TDM) to identify bridge moving loads and used singular value decomposition (SVD) to solve the noise-sensitive problem [7]. Chen et al. subsequently proposed a bridge moving load identification method based on truncated singular value decomposition methods, segmental polynomial truncation singular value decomposition method and pre-processing least squares QR decomposition method, which increases the identification accuracy of moving loads to a certain extent [8–10]. Liu et al. identified spatio-temporally coupled distributed dynamic loads using blind source separation and orthogonal matching pursuit, and obtained its spatial distribution and temporal history [11]. Wang et al. proposed a new fast-converging iterative regularization method, which successfully identified dynamic loads on stochastic structures [12]. Liu et al. proposed a power spectral density identification method for steady-state random excitation, considering the impact of multisource uncertainty, used a two-step weighted regularization strategy and response superposition-decomposition principle, and improved the accuracy and efficiency of load identification using an adaptive dimensionality reduction Chebyshev model and the first-order Taylor series [13]. He et al. proposed an L1-norm regularization load identification method based on redundant extended cosine dictionaries, which

Technical Editor: Ehsan Noroozinejad Farsangi.

✉ Linjun Wang
ljwang2006@126.com

¹ Hubei Key Laboratory of Hydroelectric Machinery Design and Maintenance, College of Mechanical and Power Engineering, China Three Gorges University, Yichang 443002, Hubei, People's Republic of China

efficiently identifies complex dynamic loads with good noise resistance [14]. Chen et al. proposed a new method for identifying dynamic loads at the interface between spacecraft and rocket using BP neural network, which further optimized the accuracy of identifying dynamic loads at the interface [15]. Li et al. combined the extended Kalman filter method with the least squares estimation method to identify unknown loads acting on time-varying structures, which more accurately estimated the parameter values of unknown loads on time-varying structures [16]. Qiao et al. used a cubic B-spline expansion function to propose a moving load identification method with high accuracy and the ability to overcome the ill-conditioning problem. This method has strong robustness to noise and uncertainty in data and can reduce estimation errors [17]. Liu et al. proposed a method to identify complex loads acting on a cantilever beam at multiple points, which reduced the data processing difficulty and improved the accuracy of load identification [18]. However, due to the complexity and uncertainty of engineering structures, existing load identification methods require strong data processing capabilities [19] and precise system response data. They are also sensitive to sensor layout. Incorrect sensor placement may also affect the accuracy of the identification results. The conjugate gradient algorithm can solve most of the above problems and has advantages such as fast computation speed and good convergence [20–23]. Wang et al. used the conjugate gradient method to identify multisource excitation forces [24]. Luo et al. introduced a bridge moving load identification technique based on an improved conjugate gradient method, which solved the noise-sensitive problem of time-domain method and the poor numerical performance of traditional conjugate gradient methods [25].

Although the moving load identification method based on the traditional conjugate gradient method is effective and reliable, it still has drawbacks such as low identification accuracy, poor noise resistance at high noise levels, and slow identification speed. Recently, the fractional-order model has become a major hotspot [26–28]. Compared with integer-order models, its advantages are excellent in describing the memory and genetic characteristics of various processes [29]. Because the order is fractional, the simulation results can more accurately describe the dynamic characteristics of the system. Based on this, this paper proposes a bridge moving load identification method based on the fractional conjugate gradient (FCG) algorithm, which avoids the selection of regularization parameters and does not introduce complex objective functions. Firstly, a mathematical model for moving load identification is established using the time-domain deconvolution method and modal superposition method. Secondly, by constructing an appropriate optimization objective function, the problem is transformed into a high-dimensional unconstrained optimization problem.

Then, the FCG method is used to solve this optimization problem to obtain the load information. Finally, the effectiveness of the proposed method is verified through numerical simulations, and the impact of noise and sensor configuration on mobile load identification is also studied.

2 Basic theory of load identification

Figure 1 shows the vehicle-bridge system model, which makes the following assumptions simplify actual engineering problems: (1) The bridge satisfies small deformation theory, Hooke's law, Navier hypothesis, and Saint-Venant's principle; (2) the bridge has uniform cross-section and constant mass per unit length; (3) the velocity of the moving load is constant, and it moves from left to right; and (4) the bridge's damping is proportional to the vibration speed.

Based on these assumptions, the displacement response $f(t)$ of the bridge under the moving load $u(x, t)$ can be expressed as:

$$\delta(x - ct)f(t) = C \frac{\partial u(x, t)}{\partial t} + \rho \frac{\partial^2 u(x, t)}{\partial t^2} + EI \frac{\partial^4 u(x, t)}{\partial t^4} \quad (2.1)$$

where: x represents the distance from the left end of the bridge; t represents time; c is the constant vehicle speed; $u(x, t)$ represents the displacement of the bridge at position x and time t ; $f(t)$ represents the moving load; C represents the viscous damping parameter; E represents the Young's modulus; I represents the moment of inertia; $\delta(x - ct)$ represents the Dirac δ function; and ρ represents the density of the beam.

Using modal superposition method and time-domain deconvolution method, we can obtain the structural response:

$$u(x, t) = \sum_n^{\infty} \frac{2}{L\rho\omega_n^d} \sin \frac{\pi nx}{L} \times \int_0^t e^{-\xi_n \omega_n (t-\tau)} \sin [\omega_n^d (t - \tau)] \sin \frac{\pi n c \tau}{L} f(\tau) d\tau, \quad (2.2)$$

in which, n represents the modal order; L represents the bridge span; $\xi_n = \frac{C}{2\rho\omega_n}$; $\omega_n = \frac{n^2 \pi^2}{L^2} \sqrt{\frac{EI}{\rho}}$; $\omega_n^d = \omega_n \sqrt{1 - \xi_n^2}$;

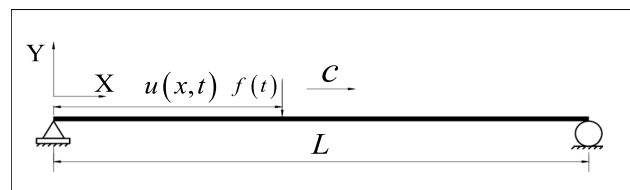


Fig. 1 The model diagram of vehicle-bridge system

and τ is the integration variable. The bridge bending moment response $m(x, t)$ and acceleration response $a(x, t)$ can be, respectively, obtained from the displacement response $u(x, t)$, as follows:

$$m(x, t) = -EI \frac{\partial^2 u(x, t)}{\partial x^2}, a(x, t) = \frac{d^2 u(x, t)}{dt^2}, \tag{2.3}$$

where

$$\frac{\partial^2 u(x, t)}{\partial x^2} = \sum_{n=1}^{\infty} -\frac{2\pi^2 n^2}{L^3 \rho \omega_n^d} \sin \frac{\pi n x}{L} \int_0^t e^{-\xi_n \omega_n (t-\tau)} \sin [\omega_n^d (t-\tau)] \sin \frac{\pi n c \tau}{L} f(\tau) d\tau, \tag{2.4}$$

$$\frac{d^2 u(x, t)}{dt^2} = \sum_{n=1}^{\infty} \frac{2}{L \rho} \sin \frac{\pi n x}{L} \left[\sin \frac{\pi n c \tau}{L} f(t) + \int_0^t \ddot{h}(t-\tau) f(\tau) \sin \frac{\pi n c \tau}{L} d\tau \right], \tag{2.5}$$

in which

$$\ddot{h}(t) = \frac{1}{\omega_n^d} e^{-\xi_n \omega_n t} \left\{ \left[(\xi_n \omega_n)^2 - \omega_n^2 \right] \sin (\omega_n^d t) + (-2\xi_n \omega_n \omega_n^d) \cos (\omega_n^d t) \right\}, \tag{2.6}$$

Then, we discrete (2.4) and (2.5) into a matrix form. If the acceleration response is measured separately, we can obtain

$$\ddot{u} = U \cdot f. \tag{2.7}$$

$N \times 1$ $N \times (N_k - 1)$ $(N_k - 1) \times 1$

If the bending moment response is measured separately, we can obtain

$$m = M \cdot f. \tag{2.8}$$

$(N-1) \times 1$ $(N-1) \times (N_k - 1)$ $(N_k - 1) \times 1$

If both bending moment and acceleration responses are measured simultaneously, they can be used together to identify the driving force. By scaling the variables m in (2.7) and \ddot{u} in (2.8) to non-dimensional units, we obtain

$$\begin{bmatrix} M/\|m\| \\ U/\|\ddot{u}\| \end{bmatrix} f = \begin{Bmatrix} m/\|m\| \\ \ddot{u}/\|\ddot{u}\| \end{Bmatrix} \tag{2.9}$$

in which, M and U are matrices of the vehicle-bridge system; m and \ddot{u} are matrices of bending moment and acceleration response, respectively. In the time domain, the load identification problem in (2.9) can ultimately be transformed into the following equation:

$$Af = Y, \tag{2.10}$$

in which, A represents the system matrix that is related to the vehicle-bridge parameters; Y represents the response vector

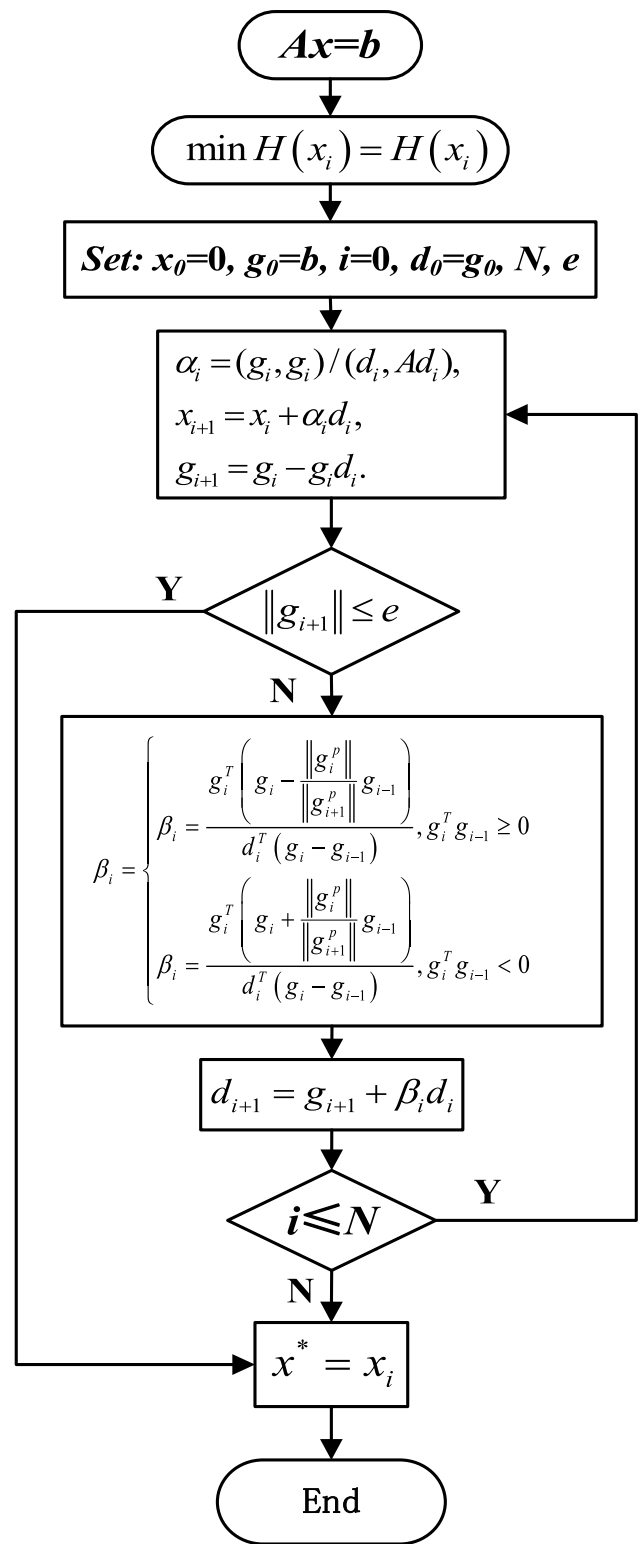


Fig. 2 The calculation flowchart of FCG method

of bending moment, acceleration response, or their combination at measurement points on the bridge; and f represents

the time series vector of moving loads. The specific forms of these matrices can be found in [7].

3 The fractional conjugate gradient method

The load identification problem can be transformed into the problem about solving matrix equation $AF = Y$. By formulating the corresponding objective function, the original issue can be converted into a high-dimensional unconstrained optimization problem:

$$\min_{w \in R^n} H(x), \tag{3.1}$$

Here, R^n represents the n-dimensional Euclidean space, and $H(x)$ is a continuously differentiable function:

$$H(x) = \frac{1}{2}x^T Ax + x^T Y, \tag{3.2}$$

The conjugate gradient method is commonly used to solve optimization problems. This method can be used to solve (3.1), and its iterative formula is expressed as

$$x_{i+1} = x_i + \alpha_i d_i, i = 0, 1, 2, \dots, \tag{3.3}$$

where i represents the number of iterations; x_i represents the solution of step i ; α_i represents the step size; d_i represents the search direction

$$d_i = \begin{cases} -g_i, & i = 1 \\ -g_i + \beta_i d_{i-1}, & i \geq 2. \end{cases} \tag{3.4}$$

We assure g_i represents the gradient of $H(x)$ at $x = x_k$, and β_i is a scalar used to adjust the direction. Different conjugate gradient algorithms use different β_i .

The scalar β_i for adjusting the search direction in the FCG method proposed in this article is given by the following formula:

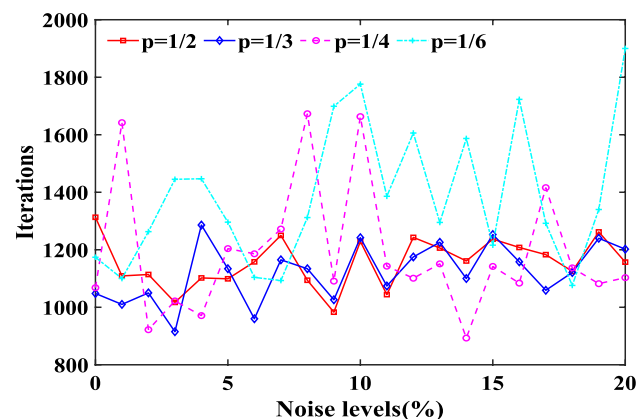


Fig. 3 Number of recognition iterations for four p values at different noise levels

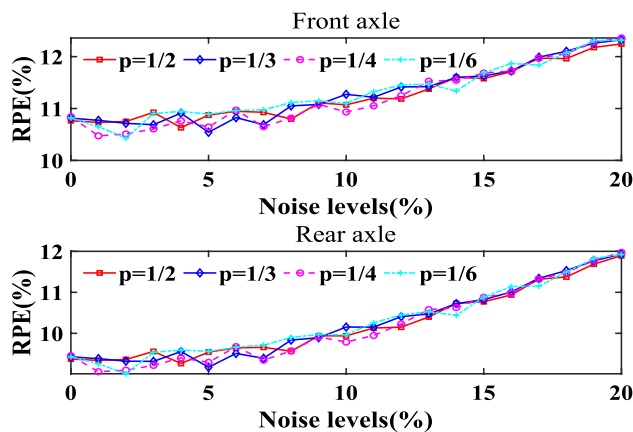


Fig. 4 The recognition accuracy of four p values at different noise levels

$$\beta_i = \begin{cases} \frac{g_i^T (g_i - \frac{\|g_i\|^p}{\|g_{i-1}\|^p} g_{i-1})}{d_i^T (g_i - g_{i-1})}, & g_i^T g_{i-1} \geq 0 \\ \frac{g_i^T (g_i + \frac{\|g_i\|^p}{\|g_{i-1}\|^p} g_{i-1})}{d_i^T (g_i - g_{i-1})}, & g_i^T g_{i-1} < 0 \end{cases} \tag{3.5}$$

where p denotes the fractional order. The maximum number of iterations in the moving force identification calculation process is set to $N = 7000$, with a precision indicator of $e = 10^{-6}$. If $N > 7000$ or $\|g_i\| \leq e$, the algorithm immediately stops iterating, yielding the identification result; otherwise, it continues iterating until a convergent solution is obtained. Based on (3.5), the detailed calculation process of the moving force identification using the proposed IFCG algorithm in this paper is illustrated in Fig. 2. The fundamental steps are described as follows:

- Step 1: Construct (2.7) using the time-domain deconvolution method and the modal superposition principle;
- Step 2: Formulate the objective function (3.1), transforming the problem of identifying moving loads into an unconstrained optimization problem;
- Step 3: Set initial values: $x_0 = 0, g_0 = b, i = 0, d_0 = g_0, N = 7000, e = 10^{-6}$;
- Step 4: Calculate the step size α_i using $\alpha_i = (g_i, g_i) / (d_i, A d_i)$;
- Step 5: Update x_i using (3.3);
- Step 6: Calculate the residual through $g_{i+1} = g_i - g_i d_i$; if $\|g_{i+1}\| \leq e$, the iteration ends, and the result x_i is output. Otherwise, proceed to the next step;
- Step 7: Calculate the directional scalar β_i using (3.5).
- Step 8: Update the search direction d_i using $d_{i+1} = g_{i+1} + \beta_i d_i$.
- Step 9: If $i \leq N$, end the iteration and output the result x_i ; otherwise, return to Step 4.

Table 1 Identification error of front axle moving load by four methods under three noise levels under different sensor configurations

Sensor configuration	Noise level = 5% front axle'RPE/%				Noise level = 10% front axle'RPE/%				Noise level = 15% front axle'RPE/%			
	FCG	HSCG	FRCG	RPRCG	FCG	HSCG	FRCG	RPRCG	FCG	HSCG	FRCG	RPRCG
	A14 &A12 &A34	2.42	2.40	2.56	2.40	3.78	4.07	5.93	3.98	5.93	5.75	10.74
M14 &M12 &M34	1.63	1.74	4.91	2.74	3.04	3.53	9.82	5.03	4.60	4.54	14.72	9.28
M14 &M34 &A12 &A34	2.38	1.62	4.91	2.98	3.14	3.10	9.82	5.31	4.73	4.76	14.72	8.76
M14 &M34 &M12 &A14	1.92	1.65	4.91	2.74	3.54	3.13	9.82	5.69	4.66	4.92	14.72	8.64
M14 &M12 &M34 &A12 &A14	1.65	1.70	4.91	2.58	3.35	3.05	9.81	5.55	4.54	4.76	14.72	7.91
M14 &M12 &M34 &A14 &A12 &A34	1.63	1.65	4.91	2.83	3.08	3.29	9.81	5.28	4.68	4.60	14.72	8.40

Table 2 Identification error of rear axle moving load by four methods under three noise levels under different sensor configurations

Sensor configuration	Noise level = 5% rear axle'RPE/%				Noise level = 10% rear axle'RPE/%				Noise level = 15% rear axle'RPE/%			
	FCG	HSCG	FRCG	RPRCG	FCG	HSCG	FRCG	RPRCG	FCG	HSCG	FRCG	RPRCG
	A14 &A12 &A34	2.66	2.68	2.88	2.69	5.87	6.29	7.73	6.10	9.27	9.06	12.27
M14 &M12 &M34	2.30	2.38	4.49	3.22	4.35	4.36	8.98	5.87	6.36	6.37	13.4	10.95
M14 &M34 &A12 &A34	2.28	2.33	4.49	3.53	4.36	4.38	8.98	6.18	6.50	6.53	13.47	10.29
M14 &M34 &M12 &A14	2.19	2.34	4.49	3.19	4.26	4.34	8.98	6.62	6.35	6.41	13.47	10.12
M14 &M12 &M34 &A12 &A14	2.27	2.40	4.49	3.02	4.25	4.34	8.98	6.51	6.36	6.37	13.47	9.22
M14 &M12 &M34 &A14 &A12 &A34	2.35	2.24	4.49	3.31	4.32	4.24	8.98	6.16	6.37	6.37	13.47	9.81

Table 3 Iterations of four methods for load identification at different noise levels under different sensor configurations

Sensor configuration	Noise level = 5% iterations				Noise level = 10% iterations				Noise level = 15% iterations			
	FCG	HSCG	FRCG	RPRCG	FCG	HSCG	FRCG	RPRCG	FCG	HSCG	FRCG	RPRCG
	A14 &A12 &A34	589	967	36	731	529	832	42	1012	665	1468	54
M14 &M12 &M34	757	775	6199	7000	809	1020	6654	7000	653	1133	6623	7000
M14 &M34 &A12 &A34	680	1395	5684	7000	777	1358	6080	7000	783	1942	6114	7000
M14 &M34 &M12 &A14	783	1942	6114	7000	606	759	6544	7000	618	1184	6720	7000
M14 &M12 &M34 &A12 &A14	660	1042	6350	7000	687	907	6638	7000	793	952	6690	7000
M14 &M12 &M34 &A14 &A12 &A34	671	956	6390	7000	615	881	6577	7000	743	908	6836	7000

4 Load identification and result analysis

4.1 Parameter selection and setting

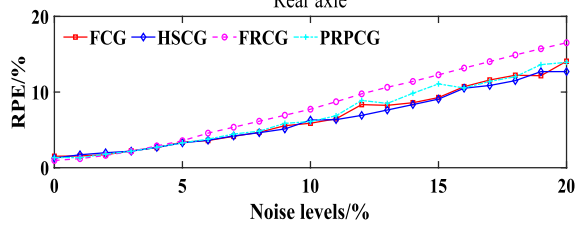
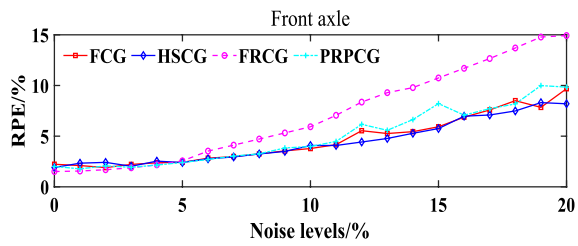
The structural parameters of the bridge model are given as follows: the flexural stiffness (EI) is $1.27 \times 10^{11} \text{ N m}^2$; the density ρ_A is $1.2 \times 10^4 \text{ kg/m}$; and the span of the beam is 40 m. The initial three resonant frequencies of the beam are 3.2 Hz, 12.8 Hz, and 28.8 Hz, respectively. The vehicle parameters are given as follows: the vehicle's moving speed is 40 m/s, the distance between the front and rear axles is 4 m, and the sampling frequency is 200 Hz.

The time history of the moving load on the front and rear axles of the vehicle is, respectively:

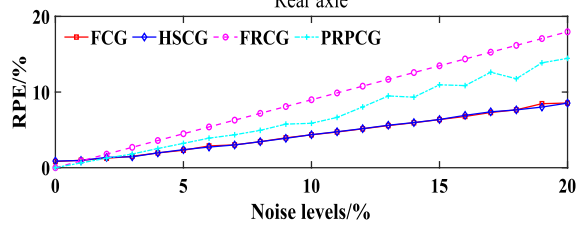
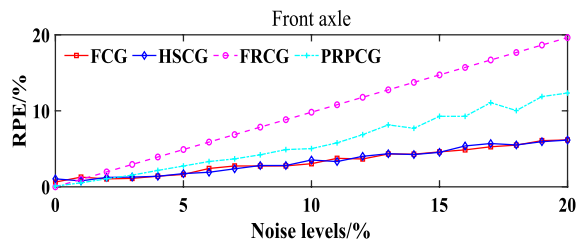
$$\begin{aligned}
 F_1(t) &= 20[1 + 0.2 \sin(10\pi t) + 0.08 \sin(40\pi t)], \\
 F_2(t) &= 20[1 - 0.2 \sin(10\pi t) + 0.08 \sin(50\pi t)].
 \end{aligned}
 \tag{4.1}$$

Considering the possible influence of errors and noise interference in the actual measurement process, this article adopts the method of simulating random noise to generate the response obtained from actual measurements:

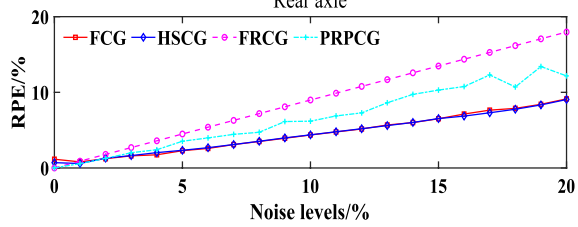
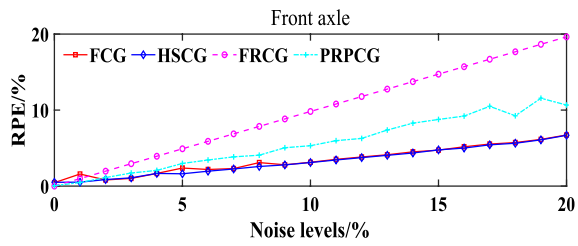
$$b_{\text{simulate}} = b_{\text{true}}(1 + nl \times N_{\text{noise}})
 \tag{4.2}$$



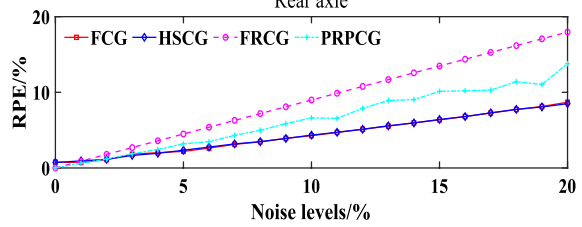
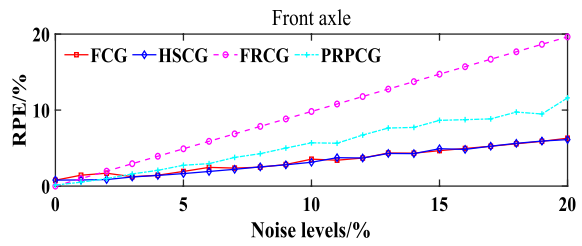
(a) A14&A12&A34



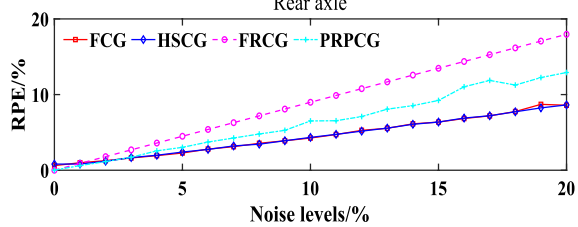
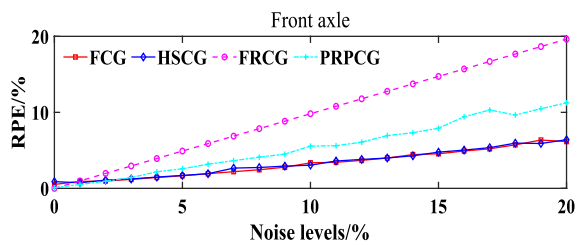
(b) M14&M12&M34



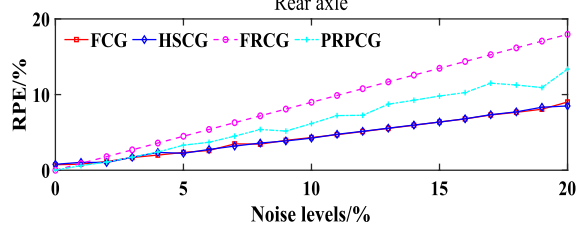
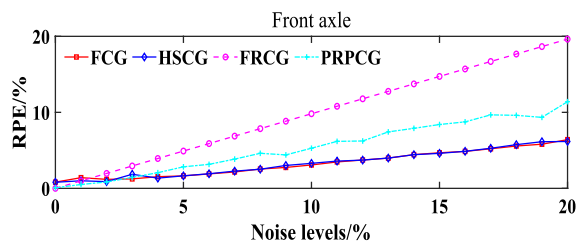
(c) M14&M34&A12&A34



(d) M14&M12&M34&A14

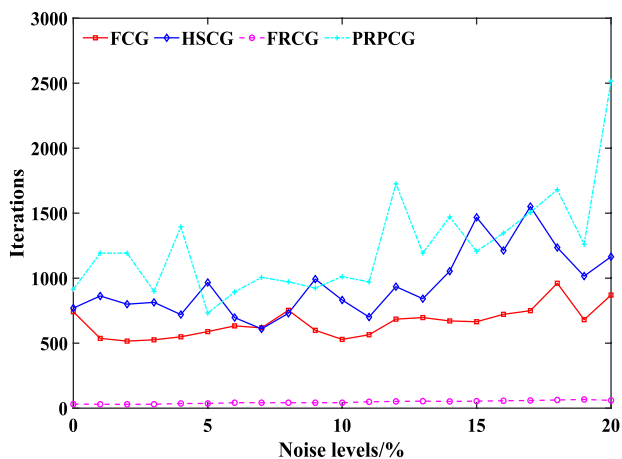


(e) M14&M12&M34&A12&A14

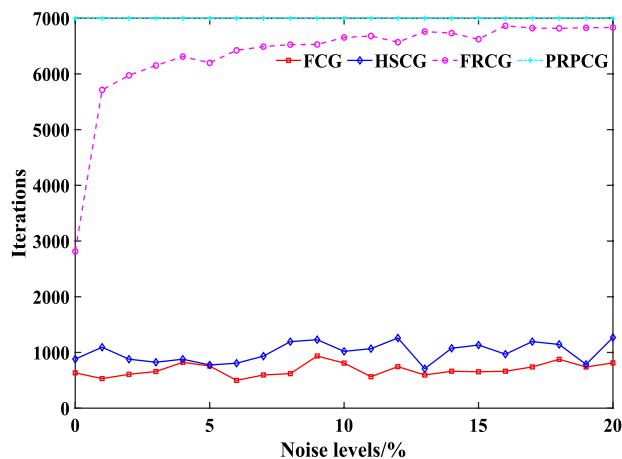


(f) M14&M12&M34&A14&A12&A34

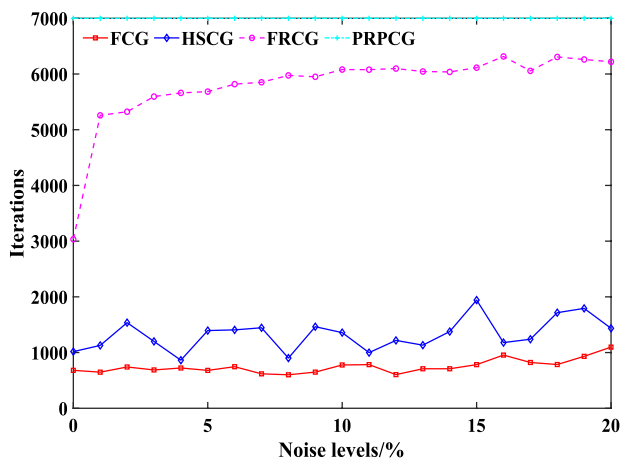
Fig. 5 The error of four kinds of conjugate gradient methods in load identification results



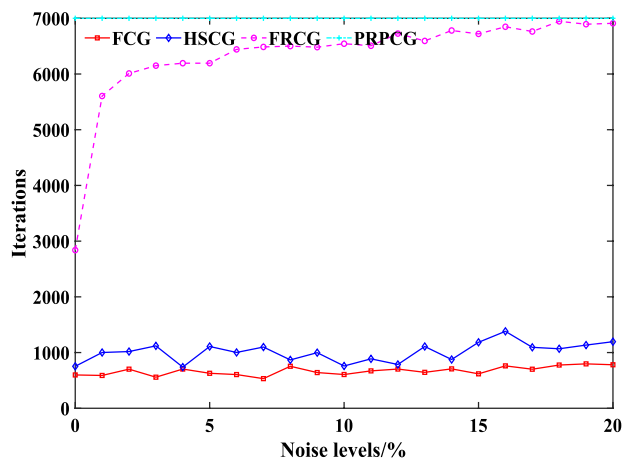
(a) $A14 \& A12 \& A34$



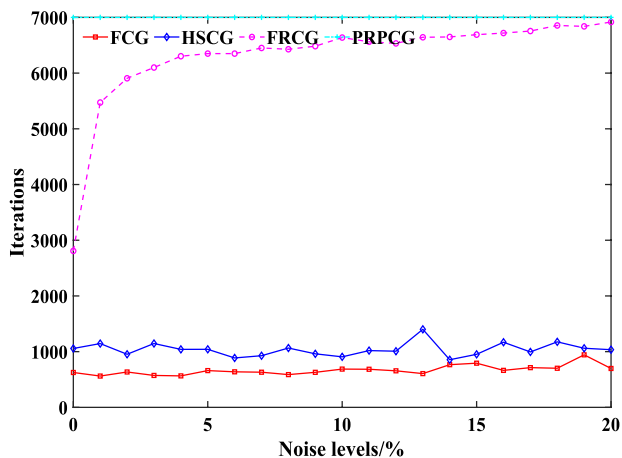
(b) $M14 \& M12 \& M34$



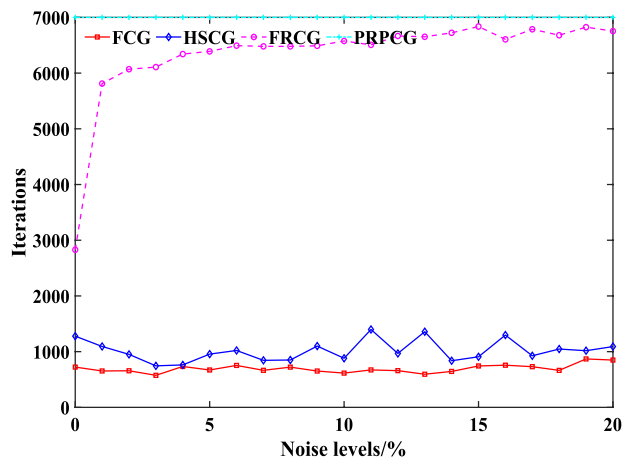
(c) $M14 \& M34 \& A12 \& A34$



(d) $M14 \& M12 \& M34 \& A14$

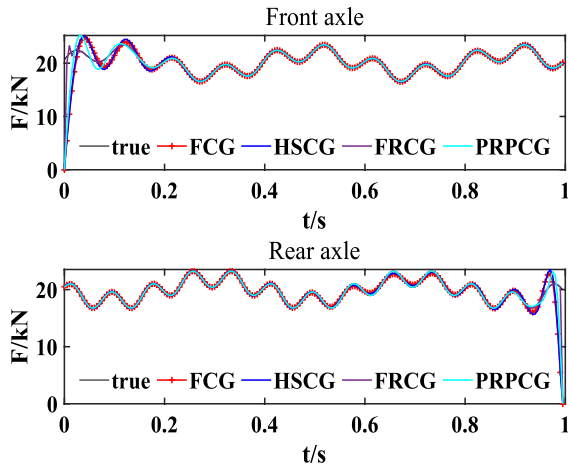


(e) $M14 \& M12 \& M34 \& A12 \& A14$

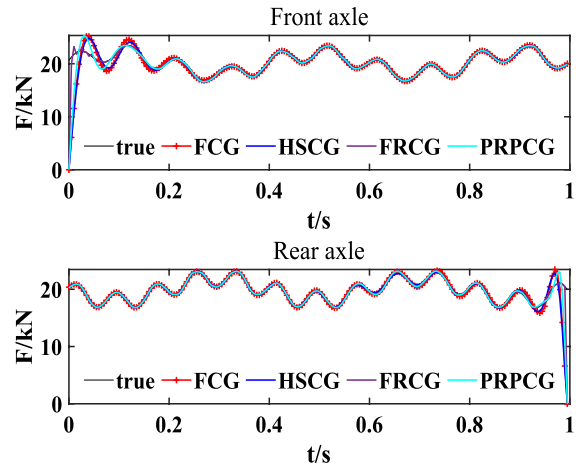


(f) $M14 \& M12 \& M34 \& A14 \& A12 \& A34$

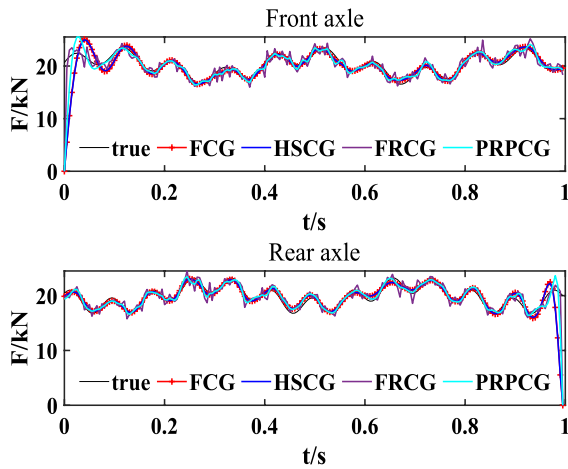
Fig. 6 The iterations of four different methods under different sensor positions



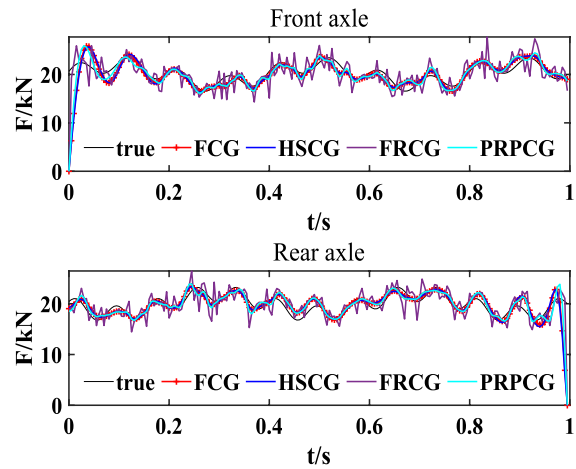
(a) 0% noise



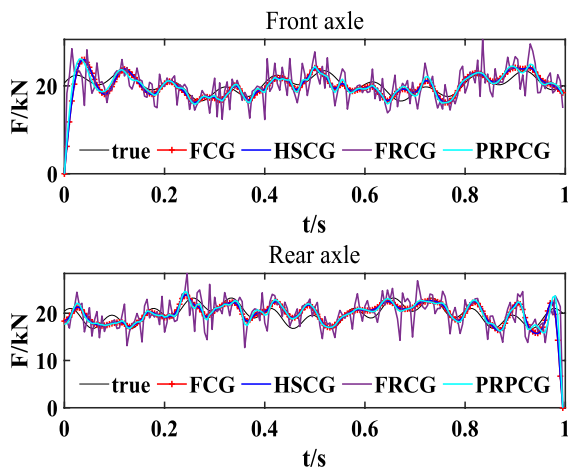
(b) 1% noise



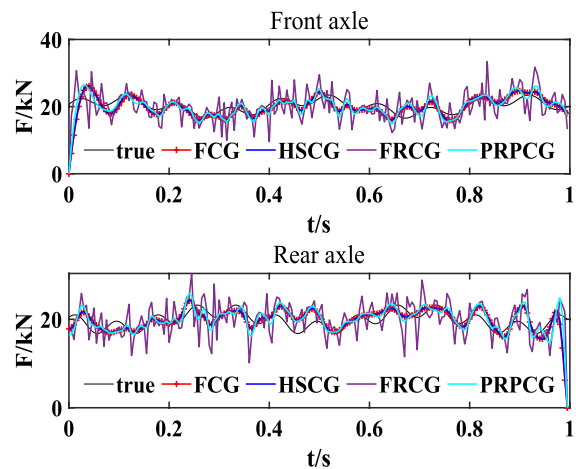
(c) 5% noise



(d) 10% noise



(e) 15% noise



(f) 20% noise

◀ **Fig. 7** The identified results of front and rear axle loads using four methods at different noise levels

in which, b_{true} represents the simulated true response; b_{simulate} represents the measured response after simulating the noise interference; nl represents the noise level; N_{noise} represents the random Gaussian white noise.

To streamline the load identification process, acceleration and bending moment sensors are strategically deployed at specific positions along the bridge span, namely at 1/4, 1/2, and 3/4 intervals. For ease of reference, M is used to represent the moment response, and A represents the acceleration response. For example, $M14$ denotes the bending moment response at the 1/4-span position, while $A34$ represents the acceleration response at the 3/4-span position, and so on for other positions. The efficiency of load identification will be assessed by measuring the number of required iterations, and the time required for each iteration will be kept constant across the different methods. A lower number of iterations will signify a more rapid load identification process.

In this study, the accuracy of the load identification process is assessed by utilizing the relative percentage error (RPE). The RPE is computed using the following formula:

$$\text{RPE} = \frac{\|F_{\text{iden}} - F_{\text{true}}\|}{\|F_{\text{true}}\|}, \quad (4.3)$$

where F_{true} is the true load, and F_{iden} is the estimated load.

The following discussion is conducted regarding the selection of the fractional order p in (3.5): under different noise levels and using a sensor configuration of $M14\&M12\&M34\&A14\&A12\&A34$, the value of p can be evaluated based on the number of accuracy of load identification and iterations results for both the front and rear axles. The specific results are shown in Figs. 3 and 4.

Based on the analysis of the load identification accuracy and iteration time in Figs. 3 and 4, it is observed that $p = 1/2$ leads to a faster load identification speed and better identification accuracy. Therefore, in the subsequent analysis, $p = 1/2$ will be selected for load identification.

4.2 The analysis of the identification results

To validate the anti-noise performance and accuracy of the proposed algorithm, this paper conducted simulation experiments on the load identification of front and rear axles by selecting six different sensor configurations and 21 noise levels (0–20% noise level, with a step of 1%). Identification error is used as the evaluation index to evaluate the precision of the load identification outcomes. Meanwhile, the FCG method is compared with other conjugate gradient methods such as Hestenes–Stiefel conjugate gradient method

(HSCG), Fletcher–Reeves conjugate gradient method (FRCG), and Polak–Ribire–Polyak conjugate gradient method (PRPCG) in terms of identification accuracy and identification speed. The specific identification results are shown in Figs. 5 and 6. The specific experimental results for the error in identifying the front and rear axis load and the number of iterations for the four methods can be found in Tables 1, 2, and 3.

As shown in Fig. 5a, when using only the acceleration to identify the load, the identification errors of the four methods are similar, but the FCG method shows slightly better identification accuracy than other methods at low noise levels. From the results in Figs. 5b and 6b, when using only the torque to identify the load, the identification errors of the FCG method and the HSCG method are much smaller than the other two methods, especially at high noise levels, and the iteration numbers of the FCG method are significantly lower than those of the HSCG method. Additionally, when combining the acceleration and torque, all methods show the stability in load identification. As shown in Figs. 5c–f and 6c–f, there were no significant jumps in identification error among these methods, indicating the stability in load identification. Furthermore, when analyzing the identification accuracy under high noise levels, the identification error of the FCG method is significantly lower than that of the FRCG method, PRPCG method, and HSCG method, and the iteration numbers required for the FCG method are much lower than the other three methods, indicating that its identification accuracy and speed are better than other methods. In conclusion, the proposed FCG method has a high identification accuracy and speed under high noise levels and is not dependent on sensor configurations.

To quantitatively analyze the identification accuracy of the FCG method, this paper chooses the sensor configuration of $M14\&M12\&M34\&A14\&A12\&A34$ and used four methods to identify the load on the front and rear axles at six different noise levels. The identification results are shown in Fig. 7.

As shown in Fig. 7, in the absence of noise, all four methods successfully achieve accurate load identification. However, as the noise level increases to 5%, the FRCG method experiences a reduction in identification accuracy, whereas the remaining three methods still accurately identify the load. Upon reaching a noise level of 10%, the FRCG method exhibits significant identification errors, while the PRPCG method demonstrates relatively smaller errors. On the other hand, the FCG method and HSCG method retain their ability to accurately identify the load. At the maximum noise level of 20%, all four methods encounter identification errors, but the FCG method exhibits comparatively smaller errors compared to the other methods. These results indicate that the FCG method has high identification accuracy and strong robustness.

5 Conclusion

- (1) This paper applies the proposed FCG to identify moving loads on bridges with six different sensor arrangements. When using bending moment and acceleration for load identification, the FRCG method and the PRPCG method achieve higher identification accuracy than the proposed FCG method at low noise level. However, at high noise level, the identification error of the proposed FCG method is lower than that of the HSCG method, the FRCG method, and the PRPCG method, indicating that the FCG method exhibits higher identification accuracy and robustness in high noise environment.
- (2) The proposed FCG method exhibits a significant advantage in identification speed, showing a faster identification speed than the FRCG method, the PRPCG method, and the HSCG method. This indicates that the FCG method performs more efficiently and quickly in handling large-scale data, which is highly beneficial for applications that require rapid processing of large amounts of data.
- (3) The load identification method proposed based on the FCG method can accurately identify moving loads on bridges and has high identification speed, robustness, and universality without sacrificing identification accuracy. The present method has broad application prospects in the practical monitoring and maintenance of bridges.

References

1. Liu J, Meng XH, Zhang DQ, Jiang C, Han X (2017) An efficient method to reduce ill-posedness for structural dynamic load identification. *Mech Syst Signal Process* 95:273–285
2. Yu B, Wu Y, Hu PM, Ding JF, Zhou HL, Wang B (2020) A non-iterative identification method of dynamic loads for different structures. *J Sound Vib* 483:115508
3. Cui WX, Jiang JH, Sun HY et al (2024) Data-driven load identification method of structures with uncertain parameters. *Acta Mech Sin* 40:523138
4. Yıldırım Ş, Esim E (2022) Investigation of dynamic response of multi-carriages double bridge overhead type crane system subjected to the moving load. *J Braz Soc Mech Sci Eng* 44:108
5. He WY, Wang Y, Ren WX (2020) Dynamic force identification based on composite trigonometric wavelet shape function. *Mech Syst Signal Process* 141:106493
6. Chen Z, Qin LF, Chan THT, Yu L (2021) A novel preconditioned range restricted GMRES algorithm for moving force identification and its experimental validation. *Mech Syst Signal Process* 155:107635
7. Law SS, Chan THT (1997) Zeng QH Moving force identification: a time domain method. *J Sound Vib* 201(1):1–22
8. Chen Z, Wei W, Yu L et al (2018) Identification of dynamic axle loads on bridge based on PPTSVD. *J Vib Meas Diagn* 38(04):727–732+871
9. Chen Z, Qin LF, Zhao SB et al (2019) Toward efficacy of piecewise polynomial truncated singular value decomposition algorithm in moving force identification. *Adv Struct Eng* 22(12):2687–2698
10. Chen Z, Wang Z, Yu L, Shao W (2018) Optimization analysis and experimental study of preconditioned least square QR-factorization for moving force identification. *J Vib Eng* 31(04):545–552
11. Liu J, Li K (2021) Sparse identification of time-space coupled distributed dynamic load. *Mech Syst Signal Process* 148:107177
12. Wang LJ, Peng YL, Xie YX et al (2021) A new iteration regularization method for dynamic load identification of stochastic structures. *Mech Syst Signal Process* 156:107586
13. Liu YR, Wang L (2023) A two-step weighting regularization method for stochastic excitation identification under multi-source uncertainties based on response superposition-decomposition principle. *Mech Syst Signal Process* 182:109565
14. He W, Xu B, Feng Z, Shi Z, Xie J, Wang W (2023) Identification of complex dynamic load using redundant extended cosine transform dictionary. *J Vib Eng* 2023:1–10
15. Chen S, Guo A, Wu S et al (2023) Dynamic load identification of satellite-rocket interface based on BP neural network. *J Vib Shock* 42(05):279–286+304
16. Li HQ, Jiang JH, Mohamed MS (2021) Online dynamic load identification based on extended Kalman filter for structures with varying parameters. *Symmetry* 13(8):1372
17. Qiao BJ, Chen XF, Xue XF et al (2015) The application of cubic B-spline location method in impact force identification. *Mech Syst Signal Process* 64:413–427
18. Liu K, Liu Q, Li J et al (2023) Load identification of composite structural based on FBG sensor and convolutional neural network. *Mater Rep* 37(01):49–55
19. Praveen KP, Balakrishnan S, Magesh A et al (2024) Numerical treatment of entropy generation and Bejan number into an electroosmotically-driven flow of Sutterby nanofluid in an asymmetric microchannel. *Numer Heat Transf Part B Fundam*. <https://doi.org/10.1080/10407790.2024.2329773>
20. Du XW, Xu CX, Ling YX (1998) Global convergence properties of the descent algorithms controlled by the FR conjugate gradient method. *J Xi'an Jiaotong Univ* 06:102–104
21. Nazareth JL (2009) Conjugate gradient method. *Wiley Interdiscip Rev Comput Stat* 1(3):348–353
22. Mohammad H, Sulaiman IM, Mamat M (2024) Two diagonal conjugate gradient like methods for unconstrained optimization. *J Ind Manag Optim* 20(1):170–187
23. Chen Z, Chan THT, Nguyen A (2018) Moving force identification based on modified preconditioned conjugate method. *J Sound Vib* 423:100–117
24. Wang LJ, Cao HP (2016) A multisource dynamic loads reconstruction method based on conjugate gradient method. *Ship Sci Technol* 38(03):69–73
25. Luo CS, Wang LJ, Xie YX et al (2024) A new conjugate gradient method for moving force identification of vehicle bridge system. *J Vib Eng Technol* 12(1):19–36
26. Gunasekaran P, Sivasubramanian R, Periyasamy K et al (2024) Adaptive cruise control system with fractional order ANFIS PD+I controller: optimization and validation. *J Braz Soc Mech Sci Eng* 46:184
27. Wang Y, Ji MZ, Zhang BY (2023) Dynamic characteristics analysis of fractional-order inerter-based suspension systems. *Noise Vib Control* 43(01):12–18
28. Arbatsofla SM, Mazinan AH, Mahmoodabadi MJ et al (2023) Fuzzy fractional-order adaptive robust feedback linearization

control optimized by the multi-objective artificial hummingbird algorithm for a nonlinear ball-wheel system. *J Braz Soc Mech Sci Eng* 45:575

29. Chen J, Shen Y, Zhang J et al (2023) Stability analysis of a fractional-order Rayleigh system with time-delayed feedback. *J Vib Shock* 42(02):16

Springer Nature or its licensor (e.g. a society or other partner) holds exclusive rights to this article under a publishing agreement with the author(s) or other rightsholder(s); author self-archiving of the accepted manuscript version of this article is solely governed by the terms of such publishing agreement and applicable law.

Publisher's Note Springer Nature remains neutral with regard to jurisdictional claims in published maps and institutional affiliations.